SUPPORTING INFORMATION

A Tetrahedral (*T*) Closed-Shell Cluster of 29 SilverAtoms & 12 Lipoate Ligands,$[Ag_{29}(R\text{-}\alpha\text{-}LA)_{12}]^{(3-)}$: Antibacterial and Antifungal Activity

Priscilla Lopez, [a] *Humberto H. Lara,* [b] *Sean Mullins,*[a] *David Black,*[a] *Heidi Ramsower,*[a] *Marcos M. Alvarez,*[a *] *Tayler L. Williams,* [c] *Xochitl Lopez-Lozano,*[a] *Hans-Christian Weissker,* [d,e] *Patricio García,* [f] *Ignacio L Garzón,*[f] *Borries Demeler,* [c] *José Luis Lopez-Ribot,* [b] *Miguel José Yacamán,* [a] *Robert L. Whetten* [a *]

[a] Department of Physics and Astronomy & [b] Department of Biology and South Texas Center for Emerging Infectious Diseases, University of Texas, San Antonio TX 78249, USA

[c] The University of Texas Health Science Center, San Antonio, Texas 78229, USA

[d] Aix Marseille University, CNRS, CINaM UMR 7325, 13288 Marseille, France
[e] European Theoretical Spectroscopy Facility (www.etsf.eu)

[f] Instituto de Física, Universidad Nacional Autónoma de México, Apartado Postal 20-364, 01000 México, D. F, México

Corresponding Authors

* marcos.alvarez@utsa.edu, robert.whetten@utsa.edu

SUPPORTING INFORMATION

Scaled Synthesis of Ag_{29}(R-α-LA_{12})clusters

Ag_{29}(R-α-LA_{12}) clusters were prepared using a scaled-up version of the preparation described by van der Linden et al. [1]

Reaction vessel: 500 mL-beaker (Pyrex/Corning) with its exterior walls covered with a double layer of aluminum foil, stirred by a 2-inch Teflon magnetic stir-bar (mixed at low setting). The vessel is capped with aluminum foil once all reactants have been mixed. All glassware is washed with dish soap and brush, rinsed with deionized water.

1. Prepare the following solutions using HPLC-grade water to be used immediately (not to be stored).

A) Dissolve 1.9 grams of (R)-alpha-lipoic acid [TCI Cat. L0207 > 98.0 %] in 100 mL of HPLC water, adding base to adjust the pH to 8-9 until the acid dissolves. We have used 1 M KOH, 30% NH_4OH, or triethylamine (TEA) for this purpose.

B) Dissolve 0.70 grams of $NaBH_4$ in 10 mL of HPLC water using a 20-mL vial. Mix capped vial using a vortex mixer.

C) Dissolve 0.29 grams of $AgNO_3$ in 10 mL of HPLC water using a 20-mL vial covered with aluminum foil; mix capped vial using vortex mixer.

D) Dissolve 1.00 grams of $NaBH_4$ in 10 mL of HPLC water using a 20-mL vial. Mix capped vial using a vortex mixer.

2. Add the first sodium borohydride solution (B) to lipoate solution (A) while stirring. React for 15 minutes with top covered with aluminum foil.

3. Add the silver nitrate solution (C) and let it react for 15 minutes with the top covered with aluminum foil.

4. Add the final sodium borohydride solution (D) and let it react for at least four hours with the top covered with aluminum foil. We normally let the reaction run overnight in a fume hood with the lights of the hood and the room switched off.

Cleaning Procedure.

Experience has shown that the clusters are susceptible to degradation when over-cleaned. The following steps are recommended to remove gross excess quantities of lipoic acid and to remove borate salts. As produced, the clusters are highly alkaline (pH ~ 10). Efforts to precipitate the clusters by lowering the pH with mild acetic acid have resulted in the degradation of clusters as judged by their change in color from orange/red to brown; the degraded clusters are not amenable to ESMS analysis. Because the solubility of lipoic acid decreases with decreasing pH, it is possible to lower the pH of the solution slightly and then extract excess lipoic acid with toluene or chloroform; however, this approach is not recommended because of the risk of degrading the clusters if too much acid is added. Instead, we found that sequential treatment with acetone first removes excess lipoic acid and then causes the clusters to precipitate leaving excess borate salts in the aqueous supernatant. We found it convenient to extract the $Ag_{29}(R\text{-}\alpha\text{-}LA_{12})$ clusters with methanol and then to evaporate the methanol to yield red-orange powders that can be stored dry for months without significant degradation as judged by ESMS spectrometry. The original precipitate that does not dissolve in methanol does dissolve in water but it yields a brown color not characteristic of clusters. (Work on characterizing and quantifying this fraction is ongoing.)

1. In 50-mL centrifuge tubes, mix and shake equal volume of acetone and clusters (at the concentrations in the synthesis above). Let the funnel undisturbed, preferably in a dark refrigerator, until white-waxy solids settle at the bottom. This process can be accelerated by centrifuging the tubes. Keep the orange/red supernatant for Step 2.

2. In a 50-mL centrifuge tube, mix the orange/red supernatant saved from Step 1 with two volumes of acetone. This time, clusters should settle out upon resting/centrifuging to yield a red/orange precipitate. The optimum volume of acetone to use may be determined by trying various ratios in a 1 mL microcentrifuge tube until enough acetone is added to cause the clusters to settle. Keep the red/orange precipitate for Step 3.

3. Extract the silver clusters from Step 3 precipitate by adding 1-2 mL of methanol and agitating in a vortex mixer; preform sequential until no more clusters are extracted as

judged by the color of the extracted liquid (two-three extractions are sufficient). Save the colored supernatant for Step 4.

4. Evaporate the methanol from the supernatant in Step 3. We have used mild UHP nitrogen flow at 0.5 SCFH for this purpose. Store the solids away from light preferably in a refrigerator.

Inhibition of MRSA and *Candida albicans* by Ag_{29}(R-α-LA_{12})clusters

Fungicidal activity in a preformed biofilm of *Candida albicans* wild-type strain SC5314 was used in this assay. Stocks of the yeast strain was stored in yeast extract-peptone-dextrose (YPD) medium combined with 15% (vol/vol) glycerol at −80°C, cells were grown on yeast extract-peptone-dextrose (YPD) agar plates at 30°C overnight. A loopful of the cells growth was inoculated into flasks (150 ml) with 20 ml of YPD broth in an orbital incubator shaker (180 rpm) and grown for 14 to 16 h at 30 °C.

Ag_{29}(R-α-LA_{12}) was tested for the antifungal activity against a preformed biofilm of *C. albicans* by a well-established phenotypic assay[2,3] at different concentrations, ranging from 1.3 to 0.0009 mg-Ag/mL in two-fold dilutions as previously reported.[3,4,5] Briefly, sterile 96-well plates were inoculated with 100 μL of 1×10^6/mL *C. albicans* cells, incubated at 37 °C for 24 h. Non-adherent cells were removed by gently washing the wells twice with PBS before adding 100 μL of different concentrations of Ag29(R-α-LA_{12}) diluted in RPMI on the well-plates and incubated for another 24 h. The plates were then washed twice with sterile PBS and processed using the XTT reduction assay (Sigma-Aldrich, St. Louis, MO) to test the efficacy of the Ag29(R-α-LA_{12}) dilutions. All experiments were performed in duplicate and repeated a minimum of three times. The IC_{50} was calculated from the dose–response nonlinear curves using a weighted nonlinear curve fitting determined by fitting the data using the software Origin 9 (Figure 2 of main text).

Bactericidal activity. Minimal inhibitory concentration (MIC) of Ag29(R-α-LA_{12}) against MRSA was tested in 96-well plates by broth microdilution in a similar manner as previously described[6] and as advised by the CLSI (2011). Briefly, single colonies of a microbiological culture were grown in selective and differential chromogenic medium plates (CHROMagar™ MRSA II). The MRSA colonies were adjusted to 1.5×10^8 CFU/mL and resuspended in Mueller-Hinton Broth (Difco Laboratories, Detroit, MI. USA) plated in 96-well microtiter plates at a final density of 5.0×10^5 CFU/well. Ag29(R-α-LA_{12}) ranged from 1.2 to 0.012 mg/mL by serial two-fold dilution. An untreated sample (without Ag29(R-α-LA_{12})) served as a control, the blank control wells contained fresh medium only. The plates were incubated at 37 °C for 18 h, and the optical density values at 600 nm were determined using a

microplate reader. All assays were carried out in duplicate, and the experiments were repeated at least three times.

Visualization of fungal biofilms and MRSA by Scanning Electron Microscopy (SEM)

For *C. albicans* biofilm and MRSA ultrastructural visualization by SEM, in 6-well plates (Corning Incorporated, Corning, NY, USA) with 6 ml of *C. albicans* at 1×10^6 cell/ml, or MRSA at 1.5×10^8 CFU/mL treated with $Ag_{29}RALA_{12}$ for 24 h at 37 °C, were washed with PBS and fixed with 4 % formaldehyde and 1 % glutaraldehyde in PBS at room temperature. Ag29(R-α-LA_{12}) were used at a concentration of 0.94 mg-Ag/mL for inhibition of the preformed biofilm of *C. albicans* and at 0.6 mg-Ag/mL for activity against MRSA. The samples were washed twice in PBS and postfixed at room temperature in 1 % osmium tetroxide (OsO_4) for 1 h. The drying process of the samples was performed with a graded ethanol series, starting with 25, 50, 75, and 95% ETOH, and absolute alcohol for 20 min. The dried specimens were then placed on copper grids to be observed with SEM in a Hitachi S-5500. Coating of the grids was achieved with 30 seconds of Gold sputter coating in the Denton DV-502A Vacuum Evaporator (Denton Vacuum, Moorestown, NJ).

Scanning Electron Microscopy

High-resolution SEM image of fungal and bacteria cells ultrastructure were achieved utilizing microscope in SE mode operating at 30.0 kV. Energy Dispersive-X-ray Spectroscopy (EDS) was achieved by using a solid state EDAX EDS detector to identify the silver signal in the treated samples. Hitachi 5500 SEM was used to collect the SE images.

Mass Spectrometry Characterization

HPLC-ESMS methods and instrumentation used have been described in detail by Black *et al*.[7]

LC Conditions (Eksigent nanoLC 2D):
MP A = ddH2O (10 mM TEAA)
MP B = Methanol (10 mM TEAA)
Gradient: 5 – 95% MP B over 20 minutes
C18 Column. Ace 300Å C18 HPLC column (0.5 mm x 150 mm, 3 μm particle size) (Hi Chrom, Theale Reading Berkshire, UK)

MS Parameters (Bruker micrOTOF time-of-flight mass spectrometer):
ESI Capillary = -4000V (Bruker keeps the spray needle tip at ground potential)
End Plate Offset = -500V (voltage applied to spray shield, value is always negative and is added to absolute voltage of the capillary)
Nebulizer = 0.4 bar
Drying Gas = 3.0 L/min
Drying Gas Temp = 250C
Capillary Exit = 35 V
Skimmer 1 = 33 V
Lens Transfer Time = 100 us
Pre-Pulse Storage Time = 40 us
m/z Range = 100 – 10000
Sum 10,000 Scans
Detector Voltage = 2400 V (up from 2000-2100 for small molecules)

AUC

Sedimentation velocity experiments were performed, using the newly released Beckman Optima AUC instrument, on samples of the silver-lipoate clusters characterized at successive stages of the purification process. (Table S1) In total six samples, taken from the different stages of the purification process, were diluted in a sodium phosphate buffer (di-basic, pH 7, 6.0 mM), in order to obtain two samples differing by 2-fold in concentration: ~ 1 OD at 330 nm (high concentration) and ~ 0.5 OD at 210 nm (low concentration, Figure S1). Each of the 12 samples was then centrifuged in standard 2-channel epon centerpieces at 40000 rpm at 20ºC for eight hours. The analysis and fitting of the data was performed using the software UltraScan III[8]. Hydrodynamic buffer corrections were estimated with UltraScan (density: 0.999 g/cm^3 and viscosity 1.002 cP). The experiments were conducted at the two concentrations to evaluate whether mass action or non-ideality was present. As the results from both concentrations were very similar, both factors were found to be negligible, so only the results from the 330 nm concentrations are reported. However, results on samples from purification stages 5 and 6 were not reported, because the data showed possible pressure effects; we associate these with the reduced cluster stability from over-purification. Sedimentation analysis was performed as outlined by Demeler.[9] A 2-dimensional spectrum analysis with 100 Monte Carlo iterations was performed to determine the effect of stochastic noise in the data, as introduced by Demeler and Brookes.[10] Heterogeneity in the sedimentation coefficient was compared among different samples using the enhanced van Holde-Weischet analysis.[11] All finite element calculations in Ultrascan were perfomed on parallel supercomputers available through the UltrasScan Science Gateway supported by NSF XSEDE grant.[12] From the analysis and fitting of the data the diffusion coefficient value of the samples was found at 14.48 x 10^{-7} cm^2/sec (Figure S2). The Stokes-Einstein equation was used in UltraScan to derive the average hydrodynamic radius of 1.49 nm (diameter of ~ 3 nm) for each sample of the silver lipoate clusters from the diffusion coefficient. Sedimentation coefficient values were also found to range from 3.8-4.6 S with the highest proportion of major species at 4.21 S. (Figure S3) By plotting the S-values a heterogeneity among the different purification stages is evident, which may be due to the excess ligand (LA) that is not covalently bonded to the silver nanoparticles and may be stripped off in the purification process (Figure S4).

Table S1: Summary of samples from various stages of purification.

Sample	Description
Purification 1	RAW $Ag_{29}LA_{12}$
Purification 2	$Ag_{29}LA_{12}$ after 1 toluene wash
Purification 3	$Ag_{29}LA_{12}$ after 1 acetone wash
Purification 4	Precipitate of $Ag_{29}LA_{12}$ after 2 acetone washes
Purification 5	Solution of $Ag_{29}LA_{12}$ from methanol extraction
Purification 6	Precipitate of $Ag_{29}LA_{12}$ from methanol extraction (after drying)

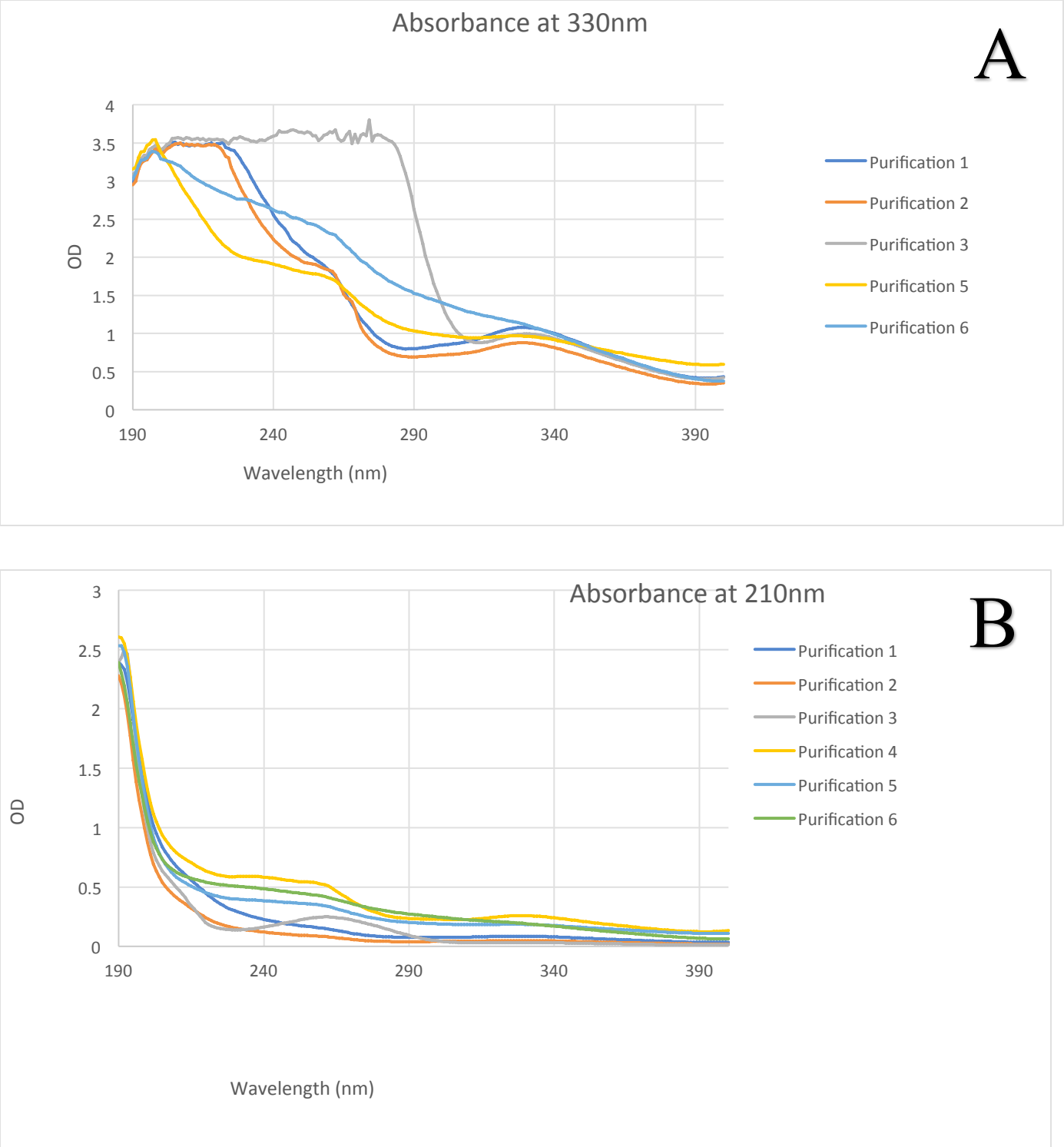

Figure S1. (a) Shown are the samples at a concentration of ~1 OD measured at 330nm (b) Samples at a concentration of ~.5 OD measured at 210nm

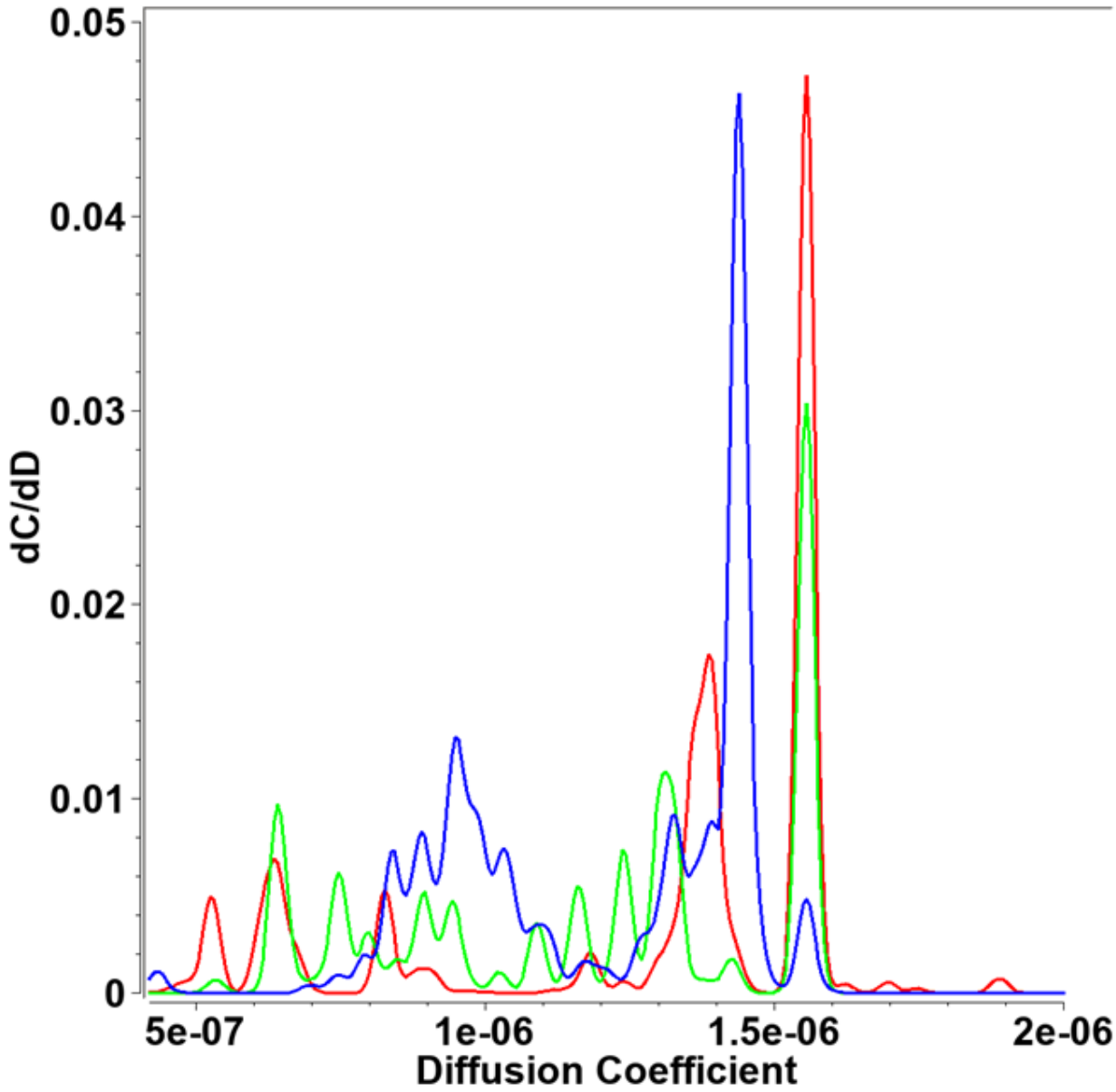

Figure S2: Diffusion coefficient distributions for purification steps 1 (green), 2 (red) and 4 (blue) from the 2DSA-Monte Carlo analysis of the AUC data, showing enrichment in a well defined species at around 1.43 x 10^{-7} cm^2/sec, which corresponds to a hydrodynamic radius of 1.5 nm.

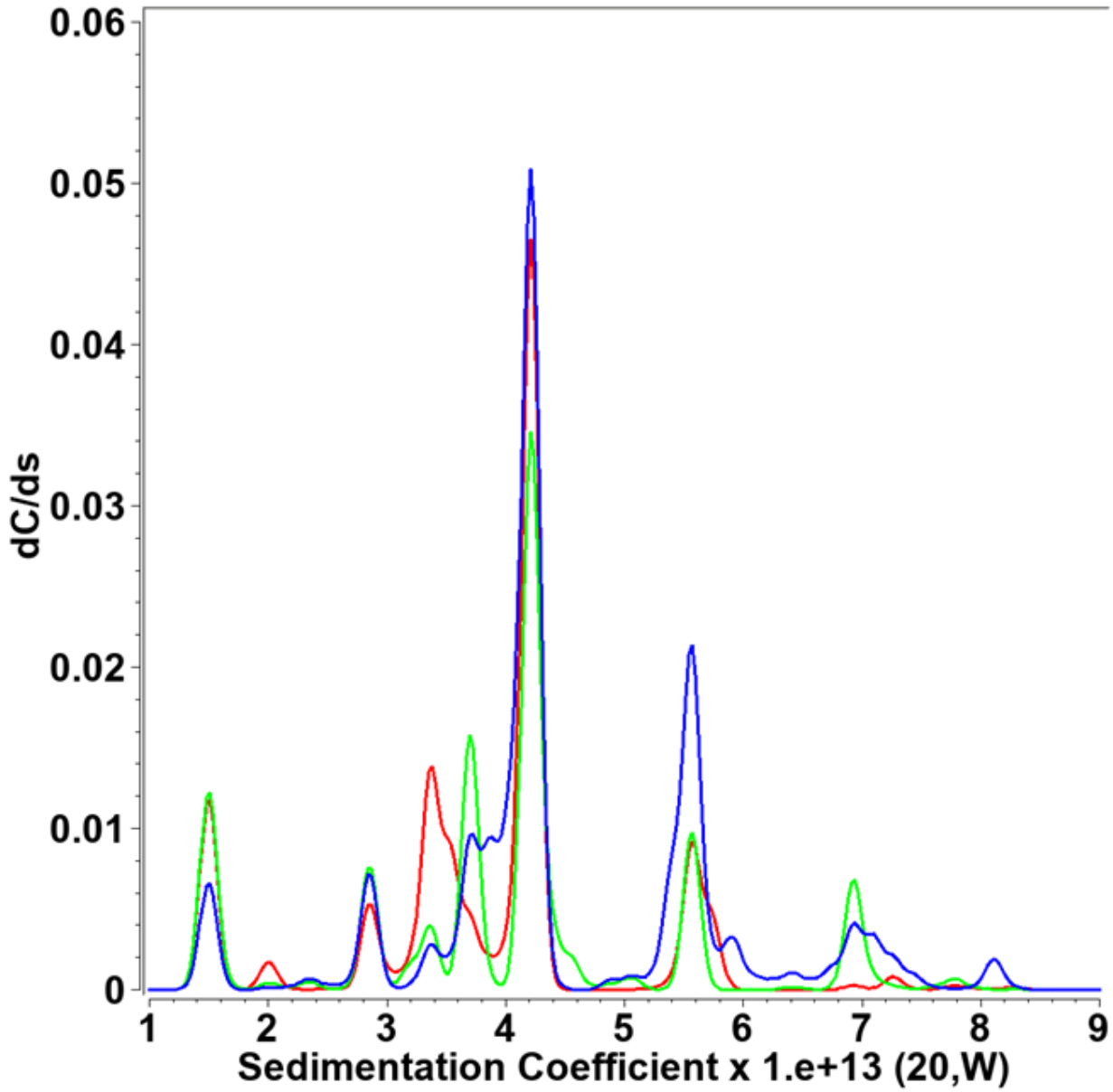

Figure S3: Sedimentation coefficient distributions for purification steps 1 (green), 2 (red) and 4 (blue) from the 2DSA-Monte Carlo analysis of the AUC data, showing enrichment in a well defined species at around 4.25 s and a secondary, less well defined species at about 5.6 s

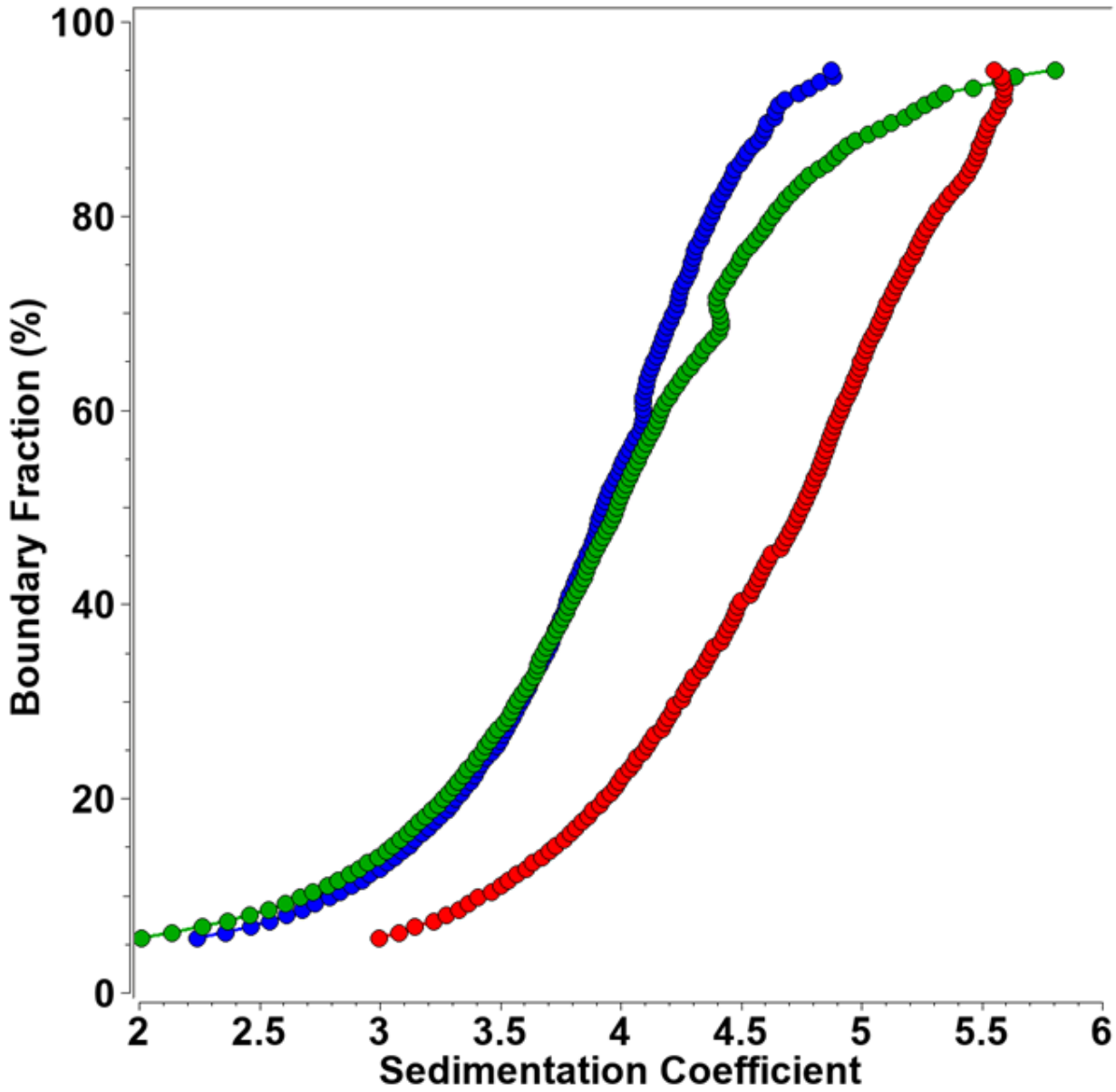

Figure S4: Diffusion-corrected sedimentation coefficient distributions from purification stages 1 (blue), 2 (green) and 4 (red) indicating moderate heterogeneity and a shift to a larger s-value for increasing purification steps.

Computational Methodology

The first-principles spin-polarized density-functional theory (DFT) calculations were performed with the SIESTA code. [13,14] The generalized-gradient approximation (GGA) exchange–correlation functional of Perdew-Burke-Ernzerhof (PBE) was used.[15] The wavefunctions were expanded in a double-ζ polarized basis set (DζP). Norm-conserving Troullier-Martins (TM) pseudopotentials (PPs) were used.[16]

A 300 Rydberg cutoff for the density integration grid and a density matrix convergence criterion of 10^{-3} eV were chosen. All the atoms were allowed to relax using the conjugate gradient minimization method until the forces were smaller than 0.01 eV/Å. A simple cubic superlattice with a cell size of 60 Å was used.

Here we report our results on two distinct models, namely

• $[Ag_{29}S_{24}P_4C_{144}H_{108}]^{-3}$: Structure morphology is maintained, tetrahedral symmetry.

• $[Ag_{29}Cl_{24}(PH_3)_4]^{-3}$: Structure morphology is maintained, tetrahedral symmetry.

Comparing the $[Ag_{29}S_{24}P_4C_{144}H_{108}]^{-3}$ and $[Ag_{29}Cl_{24}(PH_3)_4]^{-3}$ structures, we see that there is approximately a 2-5% decrease in the distance to center of mass for all atoms in the $[Ag_{29}Cl_{24}(PH_3)_4]^{-3}$ structures. We also see a difference in the band gap, 1.69 eV and 1.95 eV, for the $[Ag_{29}S_{24}P_4C_{144}H_{108}]^{-3}$ and $[Ag_{29}Cl_{24}(PH_3)_4]^{-3}$, respectively.

In order to confirm these results and put in evidence the interesting correlation between the symmetry of the systems and the degeneracies of their electronic states, the structure models were also relaxed using the density-functional theory (DFT) code VASP[17, 18] . The projector-augmented wave method (PAW)[19] and a GGA exchange-correlation functional [PW91] were employed, [20] until all forces were smaller than 0.002 eV/Å. Charge state of 3^- (three additional electrons) was used to comply with the experimental finding, which gives the expected electronic shell closing at eight (8) electrons, in accord with the SAC model. The structures obtained by this initial optimization were subsequently symmetrized in the *T*-symmetry point-group using the

SYMMOL code[21] and then re-optimized, to confirm negligible deviation from the designated symmetry.

Our results on the electronic properties for both systems are summarized in the Table below, and two figures showing the density of states (DOS) of $[Ag_{29}S_{24}P_4C_{144}H_{108}]^{-3}$ and $[Ag_{29}Cl_{24}(PH_3)_4]^{-3}$.

Table S2: Comparison side to side of the eigenvalues obtained from both, the SIESTA and VASP calculations. All states are 2-fold degenerate for spin. Clearly the obtained gaps and degeneracies are consistent. VASP calculations clarify the actual degeneracies of the energy levels of the fully symmetrized clusters.

Optimized Structure-Models for $Ag_{29}(\alpha LA)_{12}$—SIESTA-	**Optimized Structure-Models for $Ag_{29}(\alpha LA)_{12}$—VASP-**
[3-] state of complete cluster — $Ag_{29}S_{24}P_4C_{144}H_{108}$: -1.55 -1.54 -1.54 -1.52 -1.51 -1.51 -1.46 -1.42 -1.42 -1.42 **-1.39 -1.39** **HOMO-LUMO Gap = 1.70 eV** **+0.31 +0.31 +0.31** +0.51 +0.51 +0.56 0.72 0.72 0.72 0.75 0.75	**[3-] state of complete cluster — $Ag_{29}S_{24}P_4C_{144}H_{108}$:** -2.68 -2.68 -2.68 -2.63 -2.63 -2.63 -2.63 -2.51 -2.51 -2.51 **-2.49 -2.49** **HOMO-LUMO Gap = 1.77 eV** **-0.71 -0.71 -0.71** -0.57 -0.57 -0.43 -0.37 -0.37 -0.37 -0.36 -0.36 -0.36 -0.36 -0.36
[3-] state of minimal model $Ag_{29}Cl_{24}(PH_3)_4$: -1.61 -1.61 -1.61 -1.59 -1.58 -1.57 -1.57 -1.57 **-1.37 -1.37 -1.36** **HOMO-LUMO Gap = 1.95 eV** **0.58 0.59 0.59** 1.04 1.04 1.05 2.13 2.13 2.14	**[3-] state of minimal model $Ag_{29}Cl_{24}(PH_3)_4$:** -4.07 -4.07 -4.07 -4.04 -4.04 -4.04 -4.02 -4.02 **-3.83 -3.83 -3.83** **HOMO-LUMO Gap = 2.00 eV** **-1.83 -1.83 -1.83** -1.49 -1.34 -1.34 -0.63 -0.63 -0.63

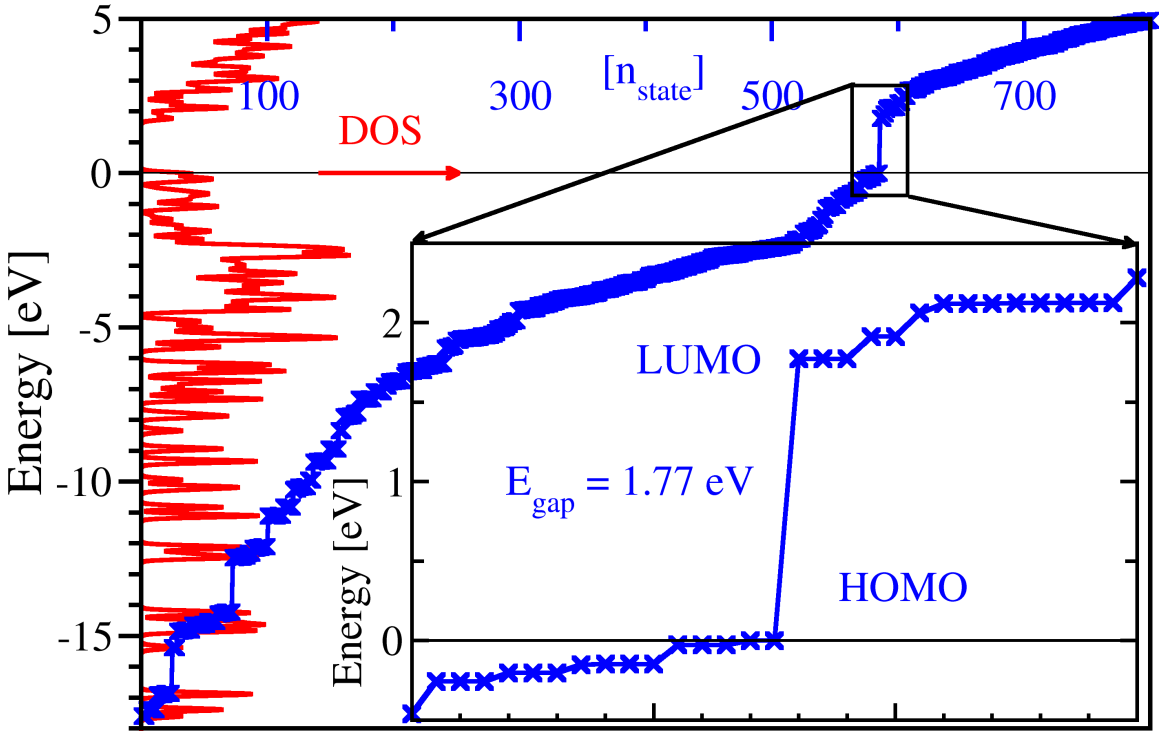

Figure S5 Electronic structure of $[Ag_{29}S_{24}P_4C_{144}H_{108}]^{-3}$. Electronic density of states (red) as well as the individual energies (blue crosses) as a function of their state number. All states are 2-fold degenerate for spin. (The HOMO state corresponds to state number 585 (2-fold degenerate times two for spin.) The inset shows a zoom of the region around the gap for the relaxed structure (blue crosses). One observes clearly the degeneracies (3-fold, 2-fold) of the states above the HOMO.

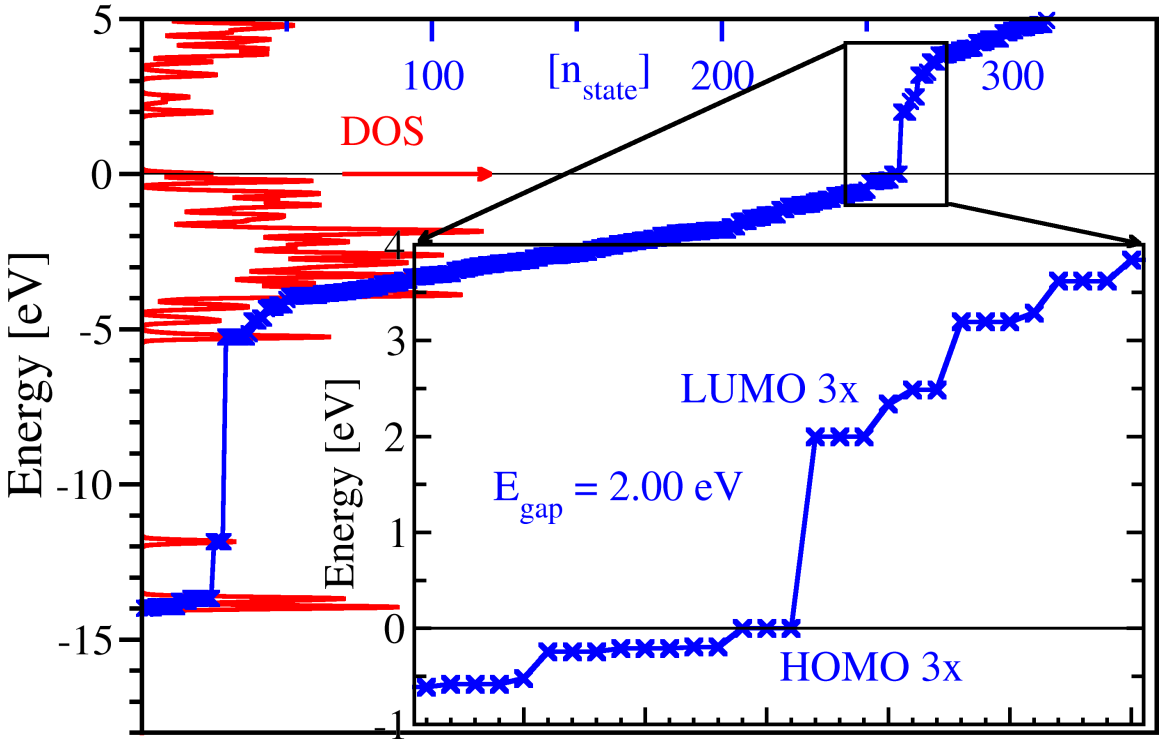

Figure S6 Electronic structure of $[Ag_{29}Cl_{24}(PH_3)_4]^{-3}$. Electronic density of states (red) as well as the individual energies (blue crosses) as a function of their state number. (The HOMO state corresponds to state number 261 (3-fold degenerate). The inset shows a zoom of the region around the gap for the relaxed structure (blue crosses). One observes clearly the degeneracies (3-fold) of the states above the HOMO.

REFERENCES

1 Linden, M. V. D.; Barendregt, A.; Bunningen, A. J. V.; Chin, P. T. K.; Thies-Weesie, D.; Groot, F. M. F. D.;Meijerink, A. Characterisation, Degradation and Regeneration of Luminescent Ag29 Clusters in Solution.Nanoscale.**2016**,*8*(47), 19901–19909.

2. Pierce, C. G.; Uppuluri, P.; Tristan, A. R.; Wormley, F. L.; Mowat, E.; Ramage, G.; Lopez-Ribot, J. L.. A Simple and Reproducible 96-Well Plate-Based Method for the Formation of Fungal Biofilms and its Application to Antifungal Susceptibility Testing. Nat. Protoc. **2008**,3, 1494–500.

3. Guisbiers, G.; Lara, H. H.; Mendoza-Cruz, R.; Naranjo, G.; Vincent, B. A.; Peralta, X. G.; Nash, K. L. Inhibition of Candida Albicans Biofilm by Pure Selenium Nanoparticles Synthesized by Pulsed Laser Ablation in Liquids. Nanomedicine Nanotechnology, Biol. Med. **2017**,13,3, 1095-1103

4.Lara, H.H.; Romero-Urbina; D.G.; Pierce, C.; Lopez-Ribot, J.L.; Arellano-Jiménez, M.J.; José-Yacamán,M. Effect of Silver Nanoparticles on Candida Albicans Biofilms: An Ultrastructural Study. J. Nanobiotechnology. **2015**, 13, 91, 1477-3155.

5. Pierce, C. G.; Saville, S. P.; Lopez-Ribot, J. L. High-content Phenotypic Screenings to Identify Inhibitors of Candida albicans Biofilm Formation and Filamentation. Pathog. Dis. **2014**,70, 423–31

6. Cardozo, V.F.; Oliveira, A.G.; Nishio, E.K.; Perugini, M.R.; Andrade, C.G.; Silveira, W.D.; Durán, N.; Andrade, G.; Kobayashi, R.K.; Nakazato, G. Antibacterial Activity of Extracellular Compounds Produced by a Pseudomonas Strain Against Methicillin-Resistant Staphylococcus aureus (MRSA) strains. Ann. Clin. Microbiol. Antimicrob. **2013**,12, 12,1-8.

7. Black, D. M.; Alvarez, M. M.; Yan, F.; Griffith, W. P.; Plascencia-Villa, G.; Bach, S. B. H.;Whetten, R. L.Triethylamine Solution for the Intractability of Aqueous Gold–Thiolate Cluster Anions: How Ion Pairing Enhances ESI-MS and HPLC of aq-Aun(pMBA)p.JPCC, **2016**,121.20,10851-0857.

8. Demeler, B.; Gorbet,G. Analytical Ultracentrifugation Data Analysis with UltraScan-III. Ch. 8, In Analytical Ultracentrifugation: Instrumentation, Software, and Applications. Eds: Uchiyama S., Stafford W. F. and T. Laue. Springer, 119-143 **(2016)**

9. Demeler,B. Methods for the Design and Analysis of Sedimentation Velocity and Sedimentation Equilibrium Experiments with Proteins. Curr. Protoc. Protein Sci. **2010**; 60:7.13:7:13.1-7.13.24.

10. Demeler, B.; Brookes, E. Monte Carlo Analysis of Sedimentation Experiments. Colloid and Polym. Sci. **2008**;286(2):129–37.

11. Demeler B;Holde, K.E.V Sedimentation Velocity Analysis of Highly Heterogeneous Systems. Anal Biochem.**2004,** 335(2):279–288.

12. Brookes, E; Demeler, B. Parallel Computational Techniques for the Analysis of Sedimentation Velocity Experiments in UltraScan. Colloid Polym. Sci. **2008**;286(2):139–48.

13 Soler, J. M.; Beltra_n, M. R.; Michaelian, K.; Garzón, I. L.; Ordejón, P.; Sánchez-Portal, D.; Artacho, E. Metallic bonding and cluster structure. Phys. Rev. B. **2000**, 61, 5771-5780.

14 Soler, J. M.; Artacho, E.; Gale, J. D.; Garca, A.; Junquera, J.; Ordejón, P.; Sánchez-Portal, D. The SIESTA method for ab initio order- N materials simulation. J. Phys: Condens Matter. **2002**, 14, 2745.

15 Perdew, J. P.; Burke, K.; Ernzerhof, M. Generalized Gradient Approximation Made Simple. Phys. Rev. Lett. **1996**, 77, 3865-3868.

16 Troullier, N.; Martins, J. L. Efficient pseudopotentials for plane-wave calculations. Phys. Rev. B. **1991**, 43, 1993-2006.

17 Kresse, G.; Hafner, J. Ab initio molecular dynamics for liquid metals. Phys. Rev. B. **1993**, 47, 558-561.

18 Kresse, G.; Furthmüller, J. Efficiency of ab-initio total energy calculations for metals and semiconductors using a plane-wave basis set. Comput. Mat. Sci. **1996**, 6, 15-50.

19 Kresse, G.; Joubert, D. From ultrasoft pseudopotentials to the projector augmented wave method. Phys. Rev. B .**1999**, 59, 1758-1775.

20 Perdew, J.P; Wang, Y .Accurate and simple analytic representation of the electron gas correlation energy,. Phys. Rev. B.**1992**, 45, 13244-13249.

21 Pilati, T.; Forni, A. SYMMOL – A program to find the maximum symmetry in an atom cluster: an upgrade. J.Appl.Crystallogr. **2000**, 33, 417.